International Journal of Nanomedicine

Dovepress
open access to scientific and medical research

Open Access Full Text Article

ORIGINAL RESEARCH

Biosynthesis of Nanoparticles with Green Tea for Inhibition of β-Amyloid Fibrillation Coupled with Ligands Analysis

Mai Zhang[1], Yan Li[1,2], Chunli Han[3], Shiying Chu[1], Peng Yu[1], Wenbo Cheng[1,2]

[1]Mass Spectrometry Application Center, Tianjin Guoke Medical Technology Development Co., Ltd, Tianjin, People's Republic of China; [2]Institute of Biomedical Engineering and Technology, Chinese Academy of Sciences (CAS), Suzhou, People's Republic of China; [3]Mass Spectrometry Application Center, Shandong CAS Intelligent Manufacturing Medical Device Technology Co., Ltd, Zaozhuang, People's Republic of China

Correspondence: Wenbo Cheng, Email chengwb@sibet.ac.cn

Background: Inhibition of amyloid β protein fragment (Aβ) aggregation is considered to be one of the most effective strategies for the treatment of Alzheimer's disease. (-)-Epigallocatechin-3-gallate (EGCG) has been found to be effective in this regard; however, owing to its low bioavailability, nanodelivery is recommended for practical applications. Compared to chemical reduction methods, biosynthesis avoids possible biotoxicity and cumbersome preparation processes.

Materials and Methods: The interaction between EGCG and Aβ42 was simulated by molecular docking, and green tea-conjugated gold nanoparticles (GT-Au NPs) and EGCG-Au NPs were synthesized using EGCG-enriched green tea and EGCG solutions, respectively. Surface active molecules of the particles were identified and analyzed using various liquid chromatography-tandem triple quadrupole mass spectrometry methods. ThT fluorescence assay, circular dichroism, and TEM were used to investigate the effect of synthesized particles on the inhibition of Aβ42 aggregation.

Results: EGCG as well as apigenin, quercetin, baicalin, and glutathione were identified as capping ligands stabilized on the surface of GT-Au NPs. They more or less inhibited Aβ42 aggregation or promoted fibril disaggregation, with EGCG being the most effective, which bound to Aβ42 through hydrogen bonding, hydrophobic interactions, etc. resulting in 39.86% and 88.50% inhibition of aggregation and disaggregation effects, respectively. EGCG-Au NPs were not as effective as free EGCG, whereas multiple thiols and polyphenols in green tea accelerated and optimized heavy metal detoxification. The synthesized GT-Au NPs conferred the efficacy of diverse ligands to the particles, with inhibition of aggregation and disaggregation effects of 54.69% and 88.75%, respectively, while increasing the yield, enhancing water solubility, and decreasing cost.

Conclusion: Biosynthesis of nanoparticles using green tea is a promising simple and economical drug-carrying approach to confer multiple pharmacophore molecules to Au NPs. This could be used to design new drug candidates to treat Alzheimer's disease.

Keywords: gold nanoparticles, green synthesis, (-)-epigallocatechin-3-gallate, liquid chromatography tandem triple quadrupole mass spectrometry, amyloid β protein, green tea

Introduction

Alzheimer's disease (AD) is a neurodegenerative disease with insidious onset and progressive progression. The Alzheimer's Disease International (ADI) 2018 Global Report stated that every three seconds, someone in the world will develop dementia.[1] Currently, the pathogenesis of AD is highly controversial, but the main pathological hallmark is the misfolding of extracellular amyloid β-protein (Aβ) and neurofibrillary tangles induced by intracellular tau proteins.[2,3] Consequently, inhibition of Aβ aggregation is considered to be one of the most effective strategies for the treatment of AD.

A variety of chemicals, including peptides,[4] curcumin,[5] alginate,[6] resveratrol,[7] and quercetin,[8] have been shown to inhibit Aβ fibrillation. Therein, (-)-epigallocatechin-3-gallate (EGCG), one of the most effective substances for inhibiting Aβ aggregation and promoting mature fiber disaggregation,[9–12] was achieved through the interaction of its own phenolic

Received: 4 December 2023
Accepted: 17 April 2024
Published: 14 May 2024

ring with the aromatic residues of Aβ by hydrogen bonding, aromatic stacking, and hydrophobicity.[13,14] Furthermore, in addition to chelating metal ions and scavenging free radicals,[15–17] Seidler et al revealed that EGCG could disaggregate brain-derived tau fibrils in vitro, fully validating the wide array of therapeutic potential of EGCG.[18]

However, the applicability of EGCG in humans has encountered with rather limited success largely due to its low stability, poor blood–brain barrier (BBB) permeability, and rapid metabolic clearance,[19] ultimately resulting in an absolute bioavailability of only 0.1%.[20] Accordingly, diversified forms of EGCG delivery systems have been designed in the clinical setup.[21–25] Istenič et al utilized liposomes to improve the storage stability of EGCG and further reinforced this effect again by polysaccharides such as sodium alginate and chitosan.[26] Moveover, the nano-EGCG synthesized by Debnath et al via polyaspartate-based micelles, can be 10–100-fold more efficient in inhibiting amyloid fibrillation, disintegrating matured amyloid fibrils, and reducing the cytotoxicity of amyloidogenesis.[27]

On the other hand, some nanoparticles (NPs) have also been found to inhibit amyloid fibril fibrillation, with the effect correlating with their size,[28,29] shape,[30,31] surface charge,[32,33] and hydrophobicity.[34,35] Vicente-Zurdo et al showed that Se NPs have antioxidant properties and the ability to cross BBB, and in vitro as well as in vivo studies have demonstrated the potential of Se NPs to reduce Aβ aggregation and inhibit tau hyperphosphorylation in the prevention and treatment of AD.[36] Besides, Au NPs are considered to be potentially functional particles owing to their advantages of easy functionalization and high penetration of the BBB.[37–40] For instance, the 3.3 nm Au NPs protected by D-glutathione significantly ameliorated memory deficits in AD model mice by blocking Aβ aggregation.[41] Nevertheless, the inhibitory efficiencies of the reported Au NPs are generally much lower than those of small molecules and peptide-based inhibitors,[33] accompanied by certain side effects, such as parietal calcification and urological complications,[42] which could be improved by encapsulating EGCG on Au NPs.[43] It is promising for obtaining stable, well-penetrated, biocompatible, bioavailable, and active AD therapeutic drugs,[44] by enhancing the affinity for binding to Aβ, and even the superposition of small molecule and NP effects.[45]

More interestingly, in addition to chemical reduction[46,47] and physical milling,[48,49] Au NPs can also be obtained by biosynthesis, which utilizes renewable raw materials without additional reductants, dispersants, or modifiers, as well as energy input, thus avoiding possible biotoxicity and cumbersome preparation processes.[50] During the production of green tea, the most retained component is polyphenols, of which the highest and most active is EGCG, accounts for 65% of the total catechin content.[51] In addition, reducing substances such as apigenin, baicalin, quercetin, and glutathione in green tea have also been shown to reduce the level of Aβ,[9,52–55] all of which can trigger the reduction of Au^{3+} and participate in the formation and stabilization of Au NPs. However, many uncertainties are associated with the biosynthetic method, especially because of the complexity of the green tea matrix, the inability to identify reducing agents, and to specify the active drug molecules that are liganded around the gold nucleus, which makes it difficult to meet clinical standards. Few studies have focused on the identification of ligands for biosynthesized NPs, resulting in a lag between the mechanistic studies and practical applications. Mass spectrometry (MS) has become one of the most promising methods for identifying unknown compounds, quantifying known materials, and elucidating the structure of molecules, with the advantages of high sensitivity and simultaneous detection of a wide range of substances.[56,57] Using liquid chromatography-tandem mass spectrometry (LC-MS/MS), ligand identification and reaction rate detection can be achieved.

As shown in Figure 1, to address the low bioavailability of EGCG in vivo, green tea was utilized to biosynthesize GT-Au NPs using a one-pot method under mild conditions, which is rapid, time-saving, non-toxic, and nonpolluting. After establishing and validating the LC-MS/MS assay, the presence of EGCG around the particles was determined with a maximum reaction rate of 96.69 ± 0.10%. It was also verified that functional small molecules, such as apigenin, quercetin, baicalein, and glutathione, which are commonly used for heavy metal detoxification and inhibition of Aβ42 fibrillation, were also stabilized as capping ligands around GT-Au NPs. The ability of the particles synthesized in different modes to inhibit Aβ42 aggregation and promote disaggregation was evaluated using the ThT fluorescence assay. Compared with Au NPs chemically synthesized with EGCG, GT-Au NPs showed higher yield, better dispersion, and more effective inhibition of Aβ42 fibrillation due to the presence of diversified reductants and stabilizers, with the effective rates of inhibition of aggregation and disaggregation of 54.69% and 88.75%, respectively, as compared to Aβ42 incubation alone. Based on circular dichroism (CD) and TEM analysis, this may be attributed to the fact that GT-Au NPs can maintain the initial conformation of Aβ42 to a certain extent, while hindering its transition to β-sheet. The self-

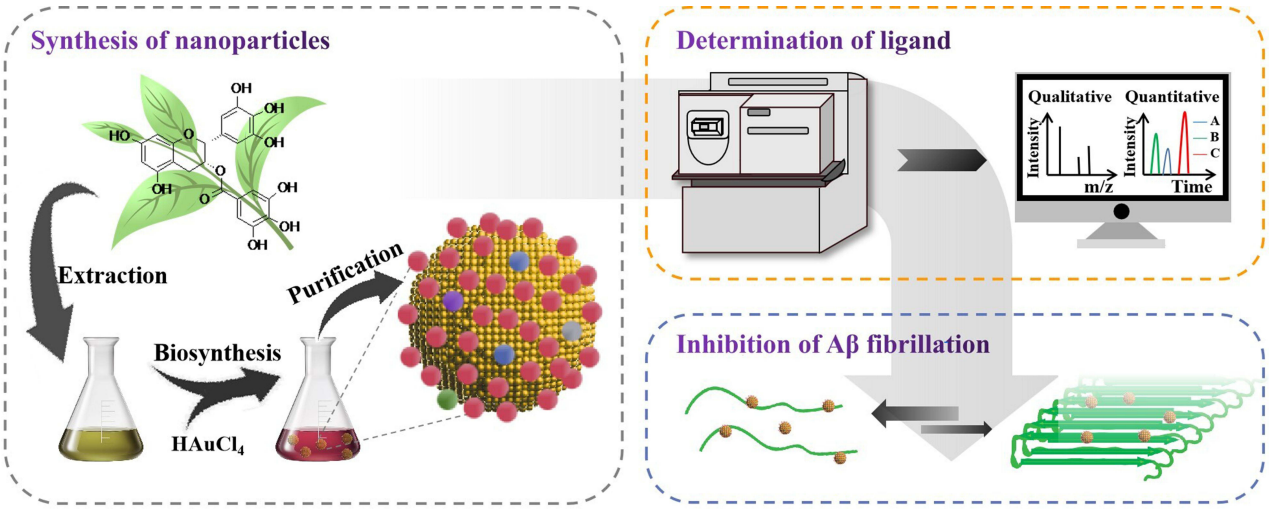

Figure 1 Diagram of green tea biosynthesis of Au NPs with ligands identified by mass spectrometry and inhibition of Aβ fibrillation.

assembly of active pharmaceutical ingredients such as EGCG can be achieved using biosynthetic techniques, thus contributing to the design and development of drugs for AD treatment and prevention.

Materials and Methods

Chemicals and Reagents

Yunwu green tea is produced in Zhejiang Province, China. $HAuCl_4 \cdot 3H_2O$ (CAS: 16961-25-4, 99.9%), and hesperidin (CAS: 520-33-2, 98%) were purchased from Aladdin (Shanghai, China). Amyloid β protein fragment 1–42 (Aβ42, 107761-42-2, 95%), EGCG (CAS: 989-51-5, 98%), quercetin (CAS: 117-39-5), apigenin (CAS: 520-36-5), reduced glutathione (CAS: 70-18-8, 99%), baicalin (21967-41-9, 98%), thioflavin T (CAS: 2390-54-7, 97%) and hexafluoroisopropanol (CAS: 920-66-1, 99.5%) were purchased from Macklin (Shanghai, China). Dimethyl sulfoxide (DMSO) and phosphate-buffered solution (PBS, 10 mM, pH 7.2–7.4) were obtained from Dingguo Changsheng Biotechnology Co., Ltd (Beijing, China) and Genview (Beijing, China), respectively. Isopropanol (CAS: 67-63-0, 99.9%) was purchased from Concord Technology Co., Ltd (Tianjin, China). 18.2 $M\Omega/cm^2$ water was obtained in-house using a UPH-II-20T ultrapure water manufacturing system (Sichuan, China).

Instruments

Various techniques were used to study and evaluate the synthesized nanoparticles. The Hitachi U-3010 spectrophotometer was utilized to obtain the ultraviolet visible absorption (UV-vis) spectra of GT-Au NPs at a resolution of 1 nm over a wavelength range of 440–650 nm. Transmission electron microscopy (TEM) images were obtained using a FEI Tecnai G2 F30 instrument operated at 200 kV. The samples were added to a thin carbon film on a Cu grid. Negative staining was additionally required to observe the morphology of Aβ42 samples. Dynamic Light Scattering (DLS) was used to measure the hydrodynamic diameter distribution of synthesized GT-Au NPs using a Malvern Zetasizer Nano ZS90 system. The X-ray diffraction (XRD) pattern was recorded on a Rigaku Ultima IV spectrometer equipped with Cu Kα, at the step of 0.02° over the range of 10°–80°. The X-ray photoelectron spectrum (XPS) was recorded from dried powder samples with the Thermo Scientific ESCALAB 250Xi spectrometer equipped with Al Kα ray. The Fourier transform infrared spectrum (FT-IR) was tested by a Thermo Scientific Nicolet iS20 spectrometer at a resolution of 4 cm^{-1} over the range of 400–4000 cm^{-1}.

The compounds were detected in the ESI mode on a triple quadrupole mass spectrometer QTRAP 5500 (AB Sciex, Canada, SN: AU23111005). The LC system of LC-20A (Shimadzu, Japan) equipped with a controller (SN: L20235532495), an autosampler (SN: L20445500870), a pair of binary pumps (SN: L20435505503), and a column oven (SN: L20205518521) was used for solvent delivery and sample introduction. The entire LC-MS/MS instrument was

controlled using Analyst software V1.6.3 (AB Sciex, Canada) for data acquisition and analysis. Partial experiments were carried out on our self-developed LC-MS/MS platform (LC-HTQ 2020, Tianjin Guoke Medical Technology Development Co., Ltd., China).

Simulation of Molecular Docking

The Aβ42 sequence is DAEFRHDSGY (10) EVHHQKLVFF (20) AEDVGSNKGA (30) IIGLMVGGVV (40) IA, and the initial coordinate was obtained from Model 1 of entry 6SZF in the RCSB PDB, whereas the initial coordinate of EGCG was obtained from PubChem (CID: 65064). Subsequently, a molecular docking simulation of Aβ42 with EGCG was performed using Swiss-Dock, and the conformations with the lowest Gibbs free energies were selected for analysis by Chimera. Specifically, interactions between Aβ42 and EGCG were determined via the Find Clashes/Contacts function to search for two potentially interacting atoms less than 4 Å apart. For clarity, areas outside the binding zone were removed from the structure.

Synthesis of Au NPs

Preparation of Green Tea Extract

Green tea leaves were ground into a uniform powder using a mortar and pestle. Then, 1 g of the powder was weighed into a round-bottomed flask and 10 mL of ultrapure water was added, heated at 80 °C for 10 min under reflux condensation. The mixture was then centrifuged at 14,000 rpm for 5 min, and the supernatant was filtered through a 0.22 μm filter membrane to obtain a yellow-green color mixture, which was stored in a refrigerator for future use.

Synthesis of GT-Au NPs

The brown bottle and rotor were soaked in aqua regia and washed with ultrapure water. 0.3 mL, 0.6 mL, 0.9 mL and 1.2 mL of green tea extract were added to 3 mL of 0.44 mM $HAuCl_4$ aqueous solution and supplemented with ultrapure water up to 5.4 mL (the volume ratios of green tea extract to $HAuCl_4$ were 1:10, 1:5, 3:10, and 2:5, respectively), yielding four sets of brownish-red solutions, which indicated that GT-Au NPs were generated. Subsequently, the mixture was stirred at 250 rpm for 40 min at room temperature to allow complete conversion of Au^{3+} ions into GT-Au NPs. After the reaction, it was centrifuged at 14,000 rpm for 30 min, and the precipitate was washed twice with isopropanol and then dried under a gentle stream of nitrogen gas, while supernatant was filtered through a 0.22 μm filter membrane, and stored at −80 °C, respectively.

Synthesis of EGCG-AuNPs

The brown bottle and rotor were soaked in aqua regia and washed with ultrapure water. 0.4 mL, 0.7 mL, 1.1 mL and 1.5 mL of a 3 mg/mL EGCG aqueous solution were added to 3 mL of 0.44 mM $HAuCl_4$ aqueous solution, and ultrapure water was supplemented with the volume of each group to 4.5 mL, corresponding to the four groups of measured concentrations of EGCG in the green tea extracts, respectively. There was no obvious change when it was mixed. After stirring at 250 rpm for 24 h at room temperature, a little powdery precipitate appeared, which was separated and purified according to the above steps to obtain EGCG-Au NPs and the supernatant.

Liquid Chromatography Tandem Mass Spectrometry Methodology Development and Detection

Liquid Chromatography Conditions

The chromatographic separation of EGCG from the matrix was performed using a Kinetex C18 column (Phenomenex, 3 mm × 50 mm, 2.6 μm). The column oven temperature was set to 40 °C. The sample injection volume for analysis was 10 μL, and the flow rate was 0.7 mL/min. Solution A of the mobile phase was ultrapure water and solution B was methanol. The column was eluted using 90% B for 0–3 min.

The chromatographic separation of apigenin, baicalin, quercetin, and glutathione from the supernatant matrix was performed on the aforementioned column with the same column oven temperature and injection volume, while the flow rate was changed to 0.8 mL/min. Gradient elution was adopted to reduce the sample analysis time; solution A of mobile

phase was ultrapure water and solution B was 50% acetonitrile in methanol. The column was treated with gradient elution according to the following timetable: 0–1 min (5% B), 1–6.5 min (5–10% B), 6.5–6.7 min (10–100% B), 6.7–9.3 min (100% B), 9.3–9.5 min (100–5% B), 9.5–10 min (5% B). All gradient steps were linear.

The chromatographic separation of apigenin, baicalin, quercetin, and glutathione from the matrix obtained by dissolving Au NPs in aqua regia was performed on a Shim-pack GIST-HP C18 column (Shimadzu, 2.1 mm × 100 mm, 3 μm). The column oven temperature and injection volume were the same as those described previously, and the flow rate was 0.5 mL/min. The mobile phase was ultrapure water (A) - methanol (B), and the column was treated with gradient elution according to the following timetable: 0–1.5 min (15% B), 1.5–2 min (15–90% B), 2–6 min (90% B), 6–6.5 min (90–15% B), 6.5–8 min (15% B). All gradient steps were linear.

Triple Quadrupole Mass Spectrometry Conditions

The mass spectrometer was operated using multiple reaction monitoring (MRM) in the negative ion mode. Curtain gas (20 psi), collision gas (Medium), ion source GS1 (50 psi), ion source GS2 (55 psi), ion spray voltage (−4500 V), ion source temperature (550 °C), and activated interface heater were identical for analytes. The deprotonated molecular ions and dominant product ions were chosen to quantify the target compounds. Specific parent/product ions information and optimized mass spectrometric parameters are shown in Table 1, including declustering potential (DP), entrance potential (EP), collision energy (CE), and cell exit potential (CXP). Qualitative and quantitative ion pairs were used for each compound.

Preparation of Standard Solutions

EGCG standards were dissolved and diluted with methanol and finally prepared as linear standard solutions of SW1-SW6 at different concentrations of 20, 50, 100, 200, 500, and 1000 μg/mL. The other standards were dissolved and diluted with ultrapure water to finalize the linear standard solutions of SW1-SW6 at the following concentrations (Table 2). The internal standard (IS) working solution (hesperidin) was prepared from the stock solution by dilution with methanol at a concentration of 200 ng/mL.

Table 1 Mass Spectrometric Acquisition Parameters

Compound	Precursor (m/z)	Quantifier (m/z)	DP (V)	EP (V)	CE (V)	CXP (V)
EGCG-1*	457.10	169.00	−126.21	−10.08	−23.36	−18.98
EGCG-2	457.10	125.00	−135.69	−6.03	−59.40	−9.59
Baicalin-1*	445.30	269.00	−143.05	−10.23	−30.29	−24.25
Baicalin-2	445.30	175.10	−144.26	−10.90	−17.56	−19.81
Glutathione-1*	306.10	143.00	−76.59	−7.96	−21.69	−16.69
Glutathione-2	306.10	128.00	−79.43	−9.84	−21.88	−16.24
Apigenin-1*	269.10	117.00	−157.78	−10.91	−47.30	−9.44
Apigenin-2	269.10	107.00	−171.46	−11.64	−34.71	−9.23
Quercetin-1*	301.10	179.10	−141.95	−11.03	−23.69	−14.39
Quercetin-2	301.10	121.00	−161.89	−8.92	−34.10	−10.93
Hesperidin-1*	301.10	164.00	−165.81	−8.02	−30.49	−16.97
Hesperidin-2	301.10	136.00	−163.97	−10.01	−36.27	−18.38

Note: *Quantitative ion pairs.

Table 2 Linear Standard Solution Concentration (ng/mL)

Compound	Supernatant						Au NPs					
	SW1	SW2	SW3	SW4	SW5	SW6	SW1	SW2	SW3	SW4	SW5	SW6
Baicalin	10.00	50.00	200.00	500.00	1250.00	2500.00	0.50	5.00	25.00	100.00	500.00	2500.00
Glutathione	100.00	250.00	500.00	1000.00	2500.00	10,000.00	2.50	10.00	50.00	200.00	1000.00	5000.00
Apigenin	0.20	1.00	4.00	10.00	20.00	40.00	0.02	0.10	0.40	1.00	4.00	10.00
Quercetin	5.00	25.00	100.00	250.00	500.00	1000.00	0.10	0.50	2.50	10.00	25.00	100.00

Sample Preparation

About 10 μL of sample (standard solution, reaction supernatant, or aqua regia solution after dissolving Au NPs) was added to a 2.0 mL microcentrifuge tube containing 1990 μL of 90% methanol in water, followed by 10 μL of IS working solution. The tubes were vortexed at 2500 rpm for 2 min to mix well. After adjusting the pH to 7 using NaOH, the sample was placed in the autosampler of the LC-MS/MS system for EGCG analysis. The procedure for detecting apigenin, baicalin, quercetin, and glutathione was slightly different from that described above: 100 μL of the sample was added to 900 μL of methanol.

Activity and Stability Investigation of Au NPs

Pretreatment for Amyloid Monomerization

To disrupt the aggregates of preformed Aß42 into monomers, 1 mg of Aβ42 was first dissolved in 1mL of HFIP and sonicated in a sealed vial for 30 min. After centrifugation at 14,000 rpm at a temperature of 4 °C for 20 min to remove any prior existing aggregates, the supernatant was transferred to a new tube and the solvent was removed in a gentle stream of nitrogen gas. Subsequently, an aliquot of Aβ42 was re-dissolved in 120 μL DMSO and diluted in 5.5 mL of ultrapure water.

ThT Fluorescence Assay for Inhibition of Aggregation Effectiveness

The Au NPs obtained from each group were sonicated and dissolved in 5.4 mL PBS, respectively. Aqueous solutions of EGCG, apigenin, baicalin, quercetin, and glutathione were also prepared at concentrations consistent with those measured in the green tea extract. One hundred microliters of Aβ42 solution was added to each well of a 96-well plate, followed by 10 μL of an aqueous solution of Au NPs, green tea extract, or small-molecule compounds in each of the experimental groups. The control group was supplemented with 10 μL of PBS. After incubation at 37 °C for a period of time, 10 μL of 20 μM ThT solution was added to each well and incubated for another 15 min. Fluorescence was measured using a microplate reader with excitation and emission wavelengths of 450 and 482 nm, respectively. The measurements of three parallel samples were recorded for each group, and the average data were calculated. Equally scaled-up samples were tested by negative staining TEM and CD, respectively, without ThT staining after the incubation process described above.

ThT Fluorescence Assay for Disaggregation Effectiveness

The Aβ42 solution was stirred continuously at 1000 rpm for 95 h at room temperature to prepare Aβ fibrils, and 50 μL of the resulting solution was added to each well of a 96-well plate. Subsequently, 10 μL of Au NPs, 50 μL of green tea extract, or an aqueous solution of small-molecule compounds was added, respectively, and the volume of each well was replenished to 100 μL with PBS. Fluorescence was measured using the same process described above.

CD Studies and Secondary Structure Analysis

To investigate the inhibition effect of GT-Au NPs on Aβ42 fibrillization, CD spectra were performed, by a JASCO J-1500 spectrometer. The samples were injected into a quartz cell with a path length of 1 mm and scanned at a wavelength of 190–260 nm. To avoid the interference of GT-Au NPs, the CD spectra of GT-Au NPs alone were used as the baseline to collect the spectra of the samples after mixed incubation. Protein secondary structure was analyzed using BeStel, an efficient method for determining secondary structure and identifying folding from CD spectra of proteins.

Results and Discussion

The Interaction of EGCG with Aβ42 Through Molecular Docking Simulation

To identify the binding mode of EGCG to Aβ42, we used Swiss-Dock, a widely used docking program to estimate the binding conformation of ligands to proteins and to provide information about binding energies and sites involved in the interaction. The three-dimensional models of the molecules before and after docking are shown in Figure 2. Figure 2a and b show the initial conformations of Aβ42 and EGCG, respectively, with carbon atom numbering of EGCG from Chimera. Among the multiple docking results obtained, the lowest binding energy was −7.967 kcal/mol, implying that it is the most probable conformation (Figure 2c), and the negative sign indicates that the EGCG molecule can bind well to Aβ42. However, it is worth

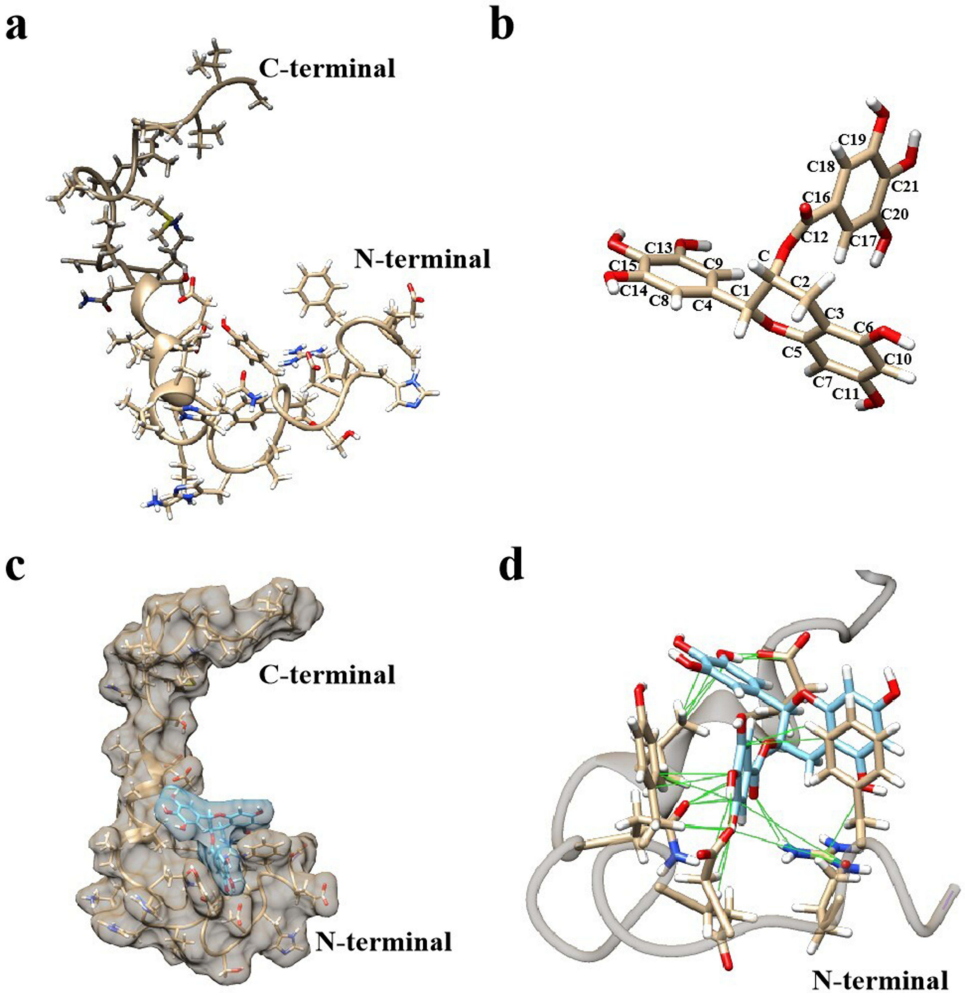

Figure 2 Three-dimensional structures and molecular docking simulation of Aβ42 and EGCG. The initial conformation of Aβ42 (**a**) and EGCG (**b**). (**c**) A graphical representation of the molecular surface of the EGCG docking with Aβ42. (**d**) Interfacial forces between Aβ42 and EGCG. The distance between the two atoms is less than 4 Å, indicated by the green solid line. EGCG was shown in cyan, and Aβ42 in beige. Oxygen atoms were labeled in red and nitrogen atoms in blue. The atomic notation were provided by Chimera and follow the PDB convention.

noting that the uncertainty in the docking calculations indicates that the importance of small differences in predicted binding affinities should not be exaggerated.[58] Subsequently, the estimated binding region was analyzed using Chimera, describing the intermolecular interactions between the specific sites spaced less than 4 Å apart (Figure 2d).

Several types of interactions are displayed in Table 3, including hydrogen bonding, weak hydrogen bonding, hydrophobic interactions, π-stacking, and salt bridges, which are the most frequent protein-ligand atomic interactions.[59] Specifically, EGCG can bind to residues Arg 5, Asp 7, Tyr 10, Glu 11, and Glu 22 via hydrogen or weak hydrogen bonds, and its three benzene rings also have π-stacking and hydrophobic interactions with residues Phe 4, Val 18, and Tyr 10. Furthermore, residue Arg 5 near the hydrophobic cavity of Aβ42 may form salt bridges with the oxygen atoms of EGCG. These results are in good agreement with those of previous studies. For instance, Gupta et al demonstrated that phenolics can bind to the hydrophobic cavity of Aβ42 protofibrils and have destabilization potential on protofibrils.[60] Li et al found that EGCG interacts with Aβ42 mainly through hydrogen bonding and hydrophobic interactions.[61] Fang et al also noted that EGCG is a good binding agent due to its ability to interact with the hydrophobic cavity of Aβ42.[9] Taken together, it is proved that EGCG does indeed bind to Aβ42 through interactions such as hydrophobicity, while hindering protein fibrillation.

Table 3 Major Interactions Between EGCG and Aβ42

Force	Atom 1 (EGCG)[a]	Atom 2 (Aβ42)[b]	Distance (Å)
π-stacking	C19	TYR 10 CE1	3.893
	C19	PHE 4 CE2	3.775
	C20	TYR 10 CD1	3.716
	C21	TYR 10 CG	3.875
	C21	TYR 10 CD1	3.476
Hydrophobic	C13	VAL 18 CG2	3.572
Hydrogen bonding	H12	GLU 22 OE2	1.937
	H16	ASP 7 OD1	2.018
	H17	ASP 7 OD1	1.848
	O6	ARG 5 HH12	2.758
Weak hydrogen bonds	O9	TYR 10 HB1	2.488
	O9	ASP 7 HB2	2.549
	O9	GLU 11 HB2	2.882
Salt bridges	O2	ARG 5 NH2	3.544
	O2	ARG 5 NHE	3.622
	O6	ARG 5 NH1	3.144

Note: [a,b]The atomic notation used in the table follows the PDB convention.

Synthesis and Characterization of Green Tea-Conjugated Gold Nanoparticles (GT-Au NPs)

Figure 3a shows the appearance of the solutions and centrifugal precipitates after the reaction of green tea extract with $HAuCl_4$ at 1:10, 1:5, 3:10, and 2:5, respectively. The color of the products differed slightly, and the solution and precipitate of the 1:10 group were more metallic, whereas the yield was significantly lower than those of the other three groups, indicating that the added green tea extract was not sufficient to completely reduce Au^{3+} and stabilize the gold nucleus. The content of green tea extract also produced small differences in the nature of the synthesized GT-Au NPs. For instance, spectrophotometric analysis of GT-AuNPs showed that characteristic surface plasmon resonance (SPR) bands were observed at 540–570 nm (Figure 3b), which confirmed the formation of Au NPs; however, the maximum absorption

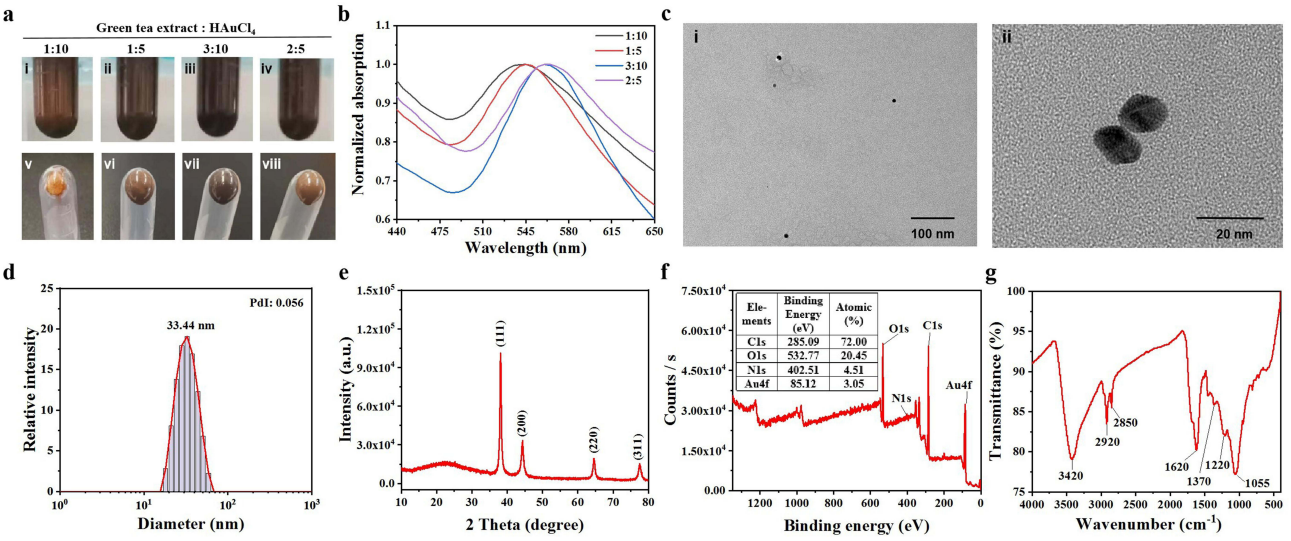

Ele-ments	Binding Energy (eV)	Atomic (%)
C1s	285.09	72.00
O1s	532.77	20.45
N1s	402.51	4.51
Au4f	85.12	3.05

Figure 3 Characterization of synthesized GT-Au NPs. (**a**) Appearance of the solution and precipitate after the reaction. The ratio of green tea extract to $HAuCl_4$ was 1:10 (i, v), 1:5 (ii, vi), 3:10 (iii, vii) and 2:5 (iv, viii). UV-visible absorption curves (**b**) and TEM (**c**) of purified GT-Au NPs. (**d**) Assessment of size distribution for GT-Au NPs measured by DLS. XRD pattern (**e**), full scan XPS survey spectrum (**f**), and FT-IR spectrum (**g**) of GT-Au NPs.

wavelengths were slightly red-shifted with an increase in green tea extract. TEM analysis showed that all groups of GT-AuNPs were nearly spherical, monodisperse, and homogeneous, with diameters of less than 20 nm (Figure 3c).

DLS was used to examine the hydrodynamic size and polydispersity of GT-Au NPs (Figure 3d), which showed an average particle size of 33.44 nm with a uniform particle size distribution (PdI=0.056). The diameter of NPs detected by DLS was always larger than that of the TEM due to the fact that the particles were flanked by a ligand coating and therefore had a solvent layer attached. XRD examination was performed to determine the exact crystal structure of the synthesized GT-Au NPs (Figure 3e). Characteristic diffraction peaks at 2θ = 38.1°, 44.3°, 64.6°, and 77.5° were observed in the spectrum, corresponding to the (111), (200), (220), and (311) planes of the face-centered cubic phases of Au (PDF #04-0784), proving the presence of Au nanocrystalline morphology. To further investigate the surface elemental composition of GT-Au NPs, XPS analysis was performed (Figure 3f). The full-scan spectrum confirmed that the GT-Au NPs were mainly composed of carbon (72.00%), oxygen (20.45%), nitrogen (4.51%) and gold (3.05%) elements. FT-IR was also performed to confirm the presence of chemical bonds on the surface of GT-Au NPs (Figure 3g). The intense absorption band at 3420 cm^{-1} characterizes the O-H stretching vibrations in alcohols and phenols. And the band at 1620 cm^{-1} can be assigned to the amide I band of the proteins released from green tea or to the C=C groups/aromatic rings. The peaks at 2920, 2850, 1370, 1220, and 1055 cm^{-1} correspond to O-H stretching vibrations of carboxylic acid, N-H stretching vibrations of amine salts, C-H stretching vibrations of aromatic amine, C-O stretching vibrations of alkyl aryl ether and C-O stretching vibrations of primary alcohol, respectively. These data suggest that polysaccharides, fatty acids, polyphenols, and reductases may be the major reducing and stabilizing agents of NPs, which is consistent with previous studies.[62–64]

Development and Validation of EGCG Detection Method by Liquid Chromatography Tandem Mass Spectrometry (LC-MS/MS)

An LC-MS/MS method was developed for accurate quantification of EGCG in green tea matrices. After comparison, Kinetex C18 chromatographic column showed a better peak shape and quantitative performance. Figure 4a shows the chromatographic signals of the target EGCG and internal standard hesperidin in the samples, with retention times of 0.610 min and 0.703 min, respectively. And the peak widths were 0.3 min and 0.2 min, respectively, with the narrow peaks favoring the detection sensitivity and accuracy. The linearity of the curve over the analytical range was assessed at six different concentrations (Figure 4b). Linear regression analysis was performed by plotting the analyte/IS peak area ratio versus concentration with a weighting of 1/(x * x), and a correlation coefficient (r) of 0.9988 was calculated, which met the method development criterion of greater than 0.990. For the determination of LLOQ, the signal-to-noise ratio (S/N) is required to be greater than 10, the accuracy deviation of 10 replicates must be within ± 15% of the nominal concentration, and the coefficient of variation (CV) for the precision analysis is required to be <20%. The validated LLOQ was fully compliant, namely, an S/N of 18.4 (Figure 4c) and an accuracy distribution in the range of 102.0–105.0% with a CV of 1.00% (n=10).

The precision and accuracy reflect the reproducibility and reliability of the assay. The CV for intra- and inter-run analytical evaluations using QC samples (QCL, QCM, QCH) should not be greater than the required 15% and the

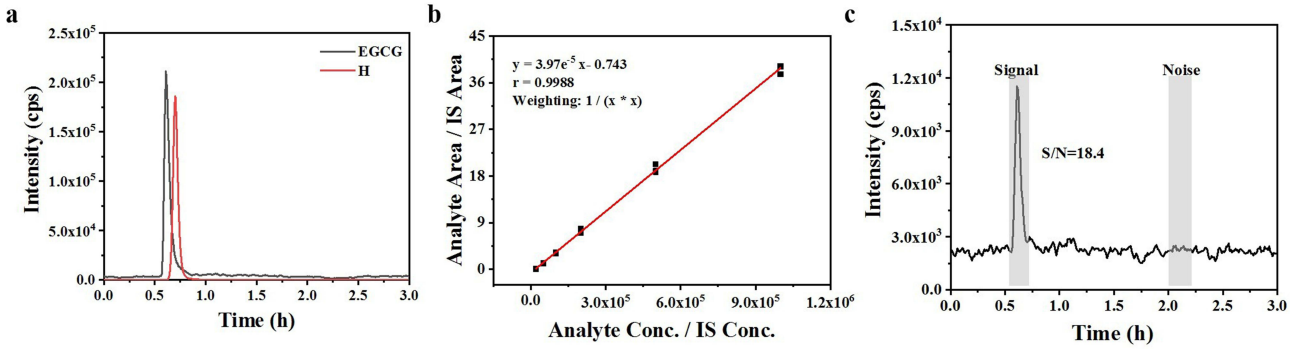

Figure 4 Methodology development for EGCG detection by mass spectrometry. (**a**) Chromatographic signals of EGCG and internal standard (quercetin, H) in standard solutions. (**b**) Linear standard curve and correlation coefficient. (**c**) Signal-to-noise (S/N) ratio at the lower limit of quantification.

accuracy of each assay must be within ± 15% of the nominal concentration. In this study, within-run precision was assessed by analyzing a single batch of five replicate QC samples in three parallel injections, and between-run precision was determined using three independent batches. QCL, QCM, and QCH were set to LLOQ, five times LLOQ, and 50% of the upper limit, respectively. The maximum value of CV was 9.24%, and accuracies were between 85.6% and 114.0%, which met the criteria for method validation, indicating extreme reproducibility and reliability of the procedure.

Impurities in the matrix may affect the ionization of the target, leading to signal enhancement or inhibition, which is known as the matrix effect (ME). The endogenous occurrence of the target and the lack of labeled internal standard prompted the use of the standard addition method as a viable alternative for evaluating ME.[65] Specifically, ME was evaluated with reference to the method of Lv et al and was calculated according to formula 1.[66] The ME (%) obtained was - 5.17%, which is within ± 15%, so that it can be considered as no significant ME.

$$ME(\%) = \left(\frac{EGCG\ concentration\ of\ spiked\ samples - Initial\ EGCG\ concentration\ of\ blank\ samples}{Spiked\ EGCG\ concentration\ detected\ in\ standard\ solution} - 1\right) \times 100 \quad (1)$$

A carryover experiment is typically applied to evaluate the interaction of continuous measurements between adjacent samples at different concentrations. In this study, carryover of EGCG was assessed by sequential injection of low-concentration (LLOQ) and high-concentration (80% upper limit of quantification) samples and calculated using Formula 2:

$$\text{Carryover}\,(\%) = (L_l - L_h)/L_l \times 100 \quad (2)$$

Where L_l and L_h represent the average measured (n=5) concentrations of the low-concentration samples injected after low- and high-concentration samples, respectively. The calculated carryover contamination of 0.10% was within ± 15%, indicating that the accuracy of the low-concentration samples would not be affected by former injection.

The Involvement of EGCG in Reduction and Stabilization of GT-Au NPs

It was achieved by detecting EGCG in the supernatant after the reaction and around GT-Au NPs. To avoid the concentration difference before and after the reaction due to the air oxidation of EGCG and other unknown factors, a control group with the same concentration without $HAuCl_4$ was set up (adjust PH to 1 with HCL, approximately equal to the acidity of the experimental group) and stirred at the same time as the experimental group. The samples were taken sometime after the reaction to detect the concentration of EGCG using LC-MS/MS. However, it has been proven that there is no significant difference in the concentration of EGCG after stirring in air, owing to its strong acidity. The results in Figure 5a show that the EGCG concentration decreased significantly after the reaction in the four experimental groups, and there was basically no EGCG residue in the 1:10 group, which is consistent with the previous description. While the

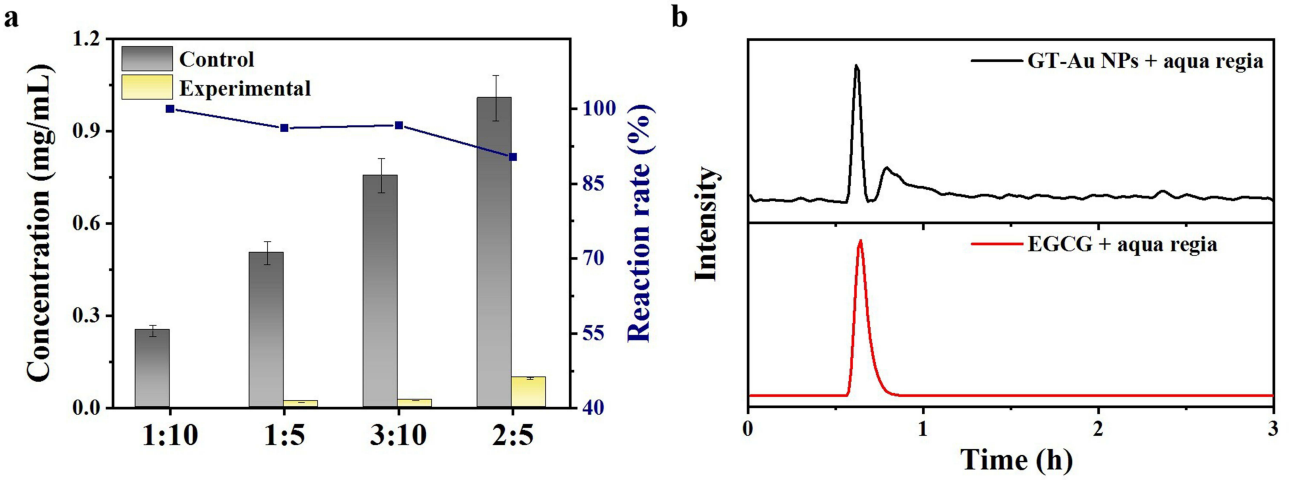

Figure 5 EGCG detection by mass spectrometry in the post-reaction supernatant (**a**) and in the GT-Au NPs precipitate (**b**). The control group was supplemented with water instead of $HAuCl_4$.

response rates of the remaining three groups were 96.14 ± 0.10%, 96.69 ± 0.10%, and 90.36 ± 0.10%, respectively, indicating that almost all of the EGCG was either consumed as a reducing agent or formulated as a stabilizer on the surface of the particles during the synthesis reaction.

To demonstrate the presence of the EGCG ligand on the surface of the GT-Au NPs, fresh aqua regia was used to fully dissolve the GT-Au NPs before LC-MS/MS detection. EGCG standard was also added to aqua regia as a control. As shown in Figure 5b, the same chromatographic peaks appeared in the supernatant of GT-Au NPs and EGCG dissolved by aqua regia and were basically the same as those mentioned above, which indicated that the structure of EGCG would not be completely destroyed by aqua regia and what is more important is that the ligand of EGCG was indeed involved in the stabilization of GT-Au NPs.

The Effect of GT-Au NPs on Aβ Fibrillation via ThT Fluorescence Assay

ThT fluorescence detection has been widely used to identify the formation of amyloid fibrils via the binding of thioflavin T to the fibrils, which leads to a prominent increase in the fluorescence quantum yield.[41] When fresh Aβ42 monomer was incubated at 37 °C ThT fluorescence was enhanced with incubation time. Remarkably, when incubating GT-Au NPs with Aβ42 monomer solution, a strong inhibitory effect on Aβ42 fibrillization was discerned, as evidenced by a 54.69% (95% Confidence Interval: 40.87–68.51%) decrease in the maximum ThT intensity compared with pure Aβ42 (Figure 6a). On the other hand, the Aβ42 fibrils obtained after vigorous stirring at room temperature for 95 h still exhibited a fluorescence intensity enhancement when incubated at 37 °C alone, while the overall fluorescence intensity showed a decreasing trend when the synthesized GT-Au NPs were added for co-incubation, resulting in an 88.78% (95% Confidence Interval: 87.17–90.40%) decrease in the final fluorescence intensity compared with that of pure Aβ42 fibrils (Figure 6b). The synthesized GT-Au NPs not only inhibited Aβ42 fibrillation, but also promoted the disaggregation of fibrotic Aβ42.

As in Figure 6c, the effect of GT-Au NPs on the conformational transition of Aβ42 was investigated using CD spectra. In the control group, aggregation of Aβ42 formed a β-sheet-rich framework. In contrast, after the addition of GT-Au NPs and incubation, the spectra showed distinct peaks characteristic of the helical structure, with two negative peaks at 208 nm and 222 nm, whereas the positive peak marked by the β-sheet configuration were significantly hindered. Further analysis of the secondary structure (Figure 6d) showed that the 48.2% content of β-sheet structure contained in

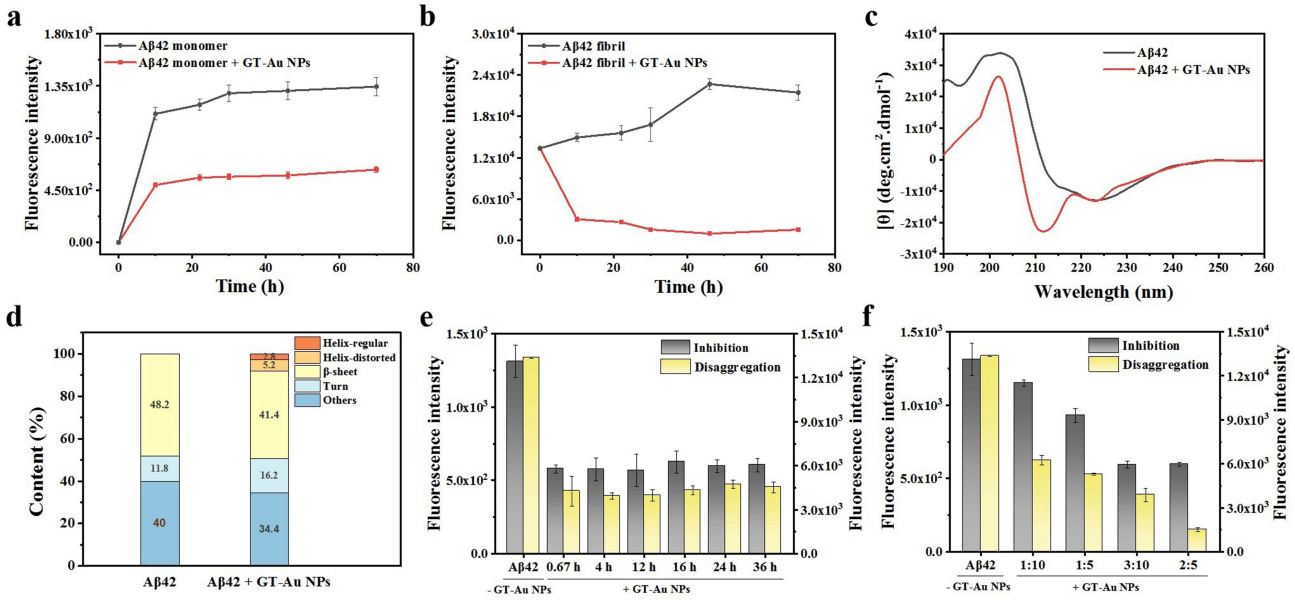

Figure 6 Effect of GT-Au NPs on Aβ42 fibrillization in vitro. ThT fluorescence assay on the aggregation inhibition (**a**) and disaggregation (**b**) of Aβ42 in the absence and presence of GT-Au NPs. (**c**) CD spectra of Aβ42 (40 μM) in the absence and presence of GT-Au NPs after co-incubation for 72 h. (**d**) Analysis of protein secondary structure. (**e**) Effect of GT-Au NPs with different synthesis times on aggregation inhibition (left axis) and degradation (right axis) of Aβ42. (**f**) Effect of GT-Au NPs with different substrate concentrations on aggregation inhibition (left axis) and degradation (right axis) of Aβ42.

the Aβ42 fibrils decreased to 41.4% after incubation with GT-Au NPs for 72 h. Meanwhile, helical structures appeared in the mixed samples, with helix-regular and helix-distorted structure contents of 2.8% and 5.2%, respectively. All of the above results indicated that GT-Au NPs may prevent the structural transition of Aβ42 from the initial helical structure to the β-sheet conformation in solution, thereby inhibiting the fibrillation, which was similar to the effect of EGCG and consistent with previous reports.[67]

Subsequently, the effects of GT-Au NPs synthesized at different times and substrate concentrations on the inhibition of Aβ42 fibrillation and promotion of fibrotic Aβ42 disaggregation were investigated. As shown in Figure 6e, there was no significant difference in the effect of the GT-Au NPs obtained at 0.67 h, 4 h, 12 h, 16 h, 24 h and 36 h, indicating that the reaction was completed within 0.67 h, which has the advantages of rapid and simple one-pot synthesis. In contrast, as shown in Figure 6f, the effect of GT-Au NPs gradually increased with the addition of the green tea extract. For the inhibition of Aβ42 fibrillation, there was no significant improvement in the effect between the 3:10 and 2:5 group, but in terms of Aβ42 degradation, the fluorescence intensity of the 2:5 group was still 61.41% (95% Confidence Interval: 42.28–80.54%) lower than that of the 3:10 group, indicating that the content of stabilizers, such as EGCG on the surface of the GT-Au NPs, would have an impact on the inhibition or disaggregation effect of the GT-Au NPs. It is speculated that the higher the content of stabilizers, the better the effect will be. This study was conducted using a reaction time of 0.67 h and a substrate concentration of 3:10 if not otherwise specified, while experiments involving disaggregation defaulted to the 2:5 group.

Synthesis and Efficacy Comparison of GT-Au NPs and EGCG-Au NPs Based on Surface Diversified Stabilizers

The complexity of the green tea substrate predetermines that the molecule involved in reduction and stabilization could not be EGCG alone. Studies have shown that coated NPs formed by the symbiotic amalgamation of NPs like gold, silver and iron oxide with natural molecules such as peptides, curcumin, drugs, catechins, etc., have great therapeutic potential for many amyloid-related diseases.[68] To further explore the molecules that might be involved in the synthetic reaction and exhibit inhibitory effects on Aβ42 fibrillation, we screened four compounds, apigenin, quercetin, baicalin, and glutathione, from the active molecules in green tea. In addition, apigenin, quercetin, and baicalin belong to the group of polyphenolic compounds, along with EGCG, which are characterized by the presence of aromatic rings and one or more phenolic rings that interact with aromatic residues in amyloid to inhibit amyloid fibrillation. Specifically, apigenin is a good Aβ-binding agent that inhibits the formation of Aβ fibrillogenesis,[9] and exhibits neuroprotective and neuroimmunomodulatory potential in vitro,[69] as well as crossing the BBB, which may be effective in improving cognitive function.[70] Similarly, quercetin could dose-dependently destabilized preformed Aβ fibrils with relatively strong activity (greater than (+)-catechin and (-)-epicatechin).[71] In addition, quercetin also possesses good BBB permeability,[70] and when NPs are functionalized with quercetin molecules, they have been shown to attenuate Aβ/tau aggregation and toxicity in cells or animal models of AD.[72] Gold-quercetin NPs proved to be far superior to quercetin in the potential to prevent inflammatory neurodegenerative diseases.[73] And the hydrolyzed product of baicalin, baicalein, has also been found to covalently binds to Aβ, hampering the aggregation and deposition of fibers,[74] showing potential for the treatment of Alzheimer's disease and Parkinson's disease.[75] Nanosizing of *S. baicalensis*'s polyphenols could improve their physicochemical properties and enhance anti-amyloidogenic and antioxidant properties.[76] While glutathione, which possesses high biocompatibility, modification ability, and water solubility, is often used as a stabilizer and detoxifier of Au NPs by encapsulating heavy metal centers.[77,78] As a tripeptide antioxidant, it can protect tissues from reactive oxygen species damage and promote penetration into the BBB due to high levels of glutathione transporters in the brain.[79] Most importantly, the surface chirality and helix structure can enantioselectively block Aβ aggregation in vitro, so that the introduction of glutathione ligand is expected to endow Au NPs with exceptional ability to inhibit Aβ fibrillation.[41] Taken together, the presence of these functional molecules would confer more marvelous physicochemical properties and clinical therapeutic perspective to GT-Au NPs, based on the fact that they are highly likely to be involved in the reaction due to their excellent reducing and chelating properties.

To identify whether the above functional molecules were involved in the reduction and stabilization of GT-Au NPs, two simultaneous detections by LC-MS/MS were established based on two matrices, namely the supernatant after the reaction and that of the GT-Au NPs dissolved in aqua regia, to achieve a better detection effect. The column type and eluent components were carefully studied to ensure improved chromatographic signals and peak shapes, and the gradient elution procedure was fine-tuned. Figure 7a and b show the chromatographic signals of the two methods for the detection of the four compounds and the internal standard hesperidin, respectively, and none of the peak widths exceeded 0.3 min, which is favorable for the detection sensitivity and accuracy. The linearity of the curve over the analytical range was assessed at six different concentrations (Table 4). The linear range of the method based on the Kinetex C18 column is more suitable for high-concentration samples, and the generally high r-value is advantageous for quantification when applied to the post-reaction supernatant assay. The method established using the Shim-pack GIST-HP C18 column, on the other hand, has a much lower LLOQ with the ability to detect several tens of pg/mL of analytes, making it more suitable for ligand detection at low concentrations. Figure 7c shows that all four compounds were detected on the GT-Au NPs, proving their involvement as ligands in the stabilization of GT-Au NPs. The supernatants of the experimental and control groups were assayed after the reaction, and the results are shown in Figure 7d. The content of all the four compounds in the 3:10 group decreased as the reaction progressed, with apigenin, baicalein, quercetin, and glutathione showing response rates of 48.53 ± 0.11%, 48.09 ± 0.13%, 73.25 ± 0.15%, and 100.00 ± 0.06%, respectively (Table 5).

The concentrations of the four compounds in the four groups of reaction solutions were examined and the reaction rates were calculated (Table 5). The highest consumption of apigenin and baicalin was basically reached in the 1:5 group, which was 3.3 ± 0.5 ng/mL and 6.0 ± 1.1 ng/mL, respectively, and the highest reaction rates were 73.33 ± 0.13% and 81.82 ± 0.16%, respectively. For quercetin, the highest consumption was reached in the 3:10 group at 212.2 ± 35.9 ng/

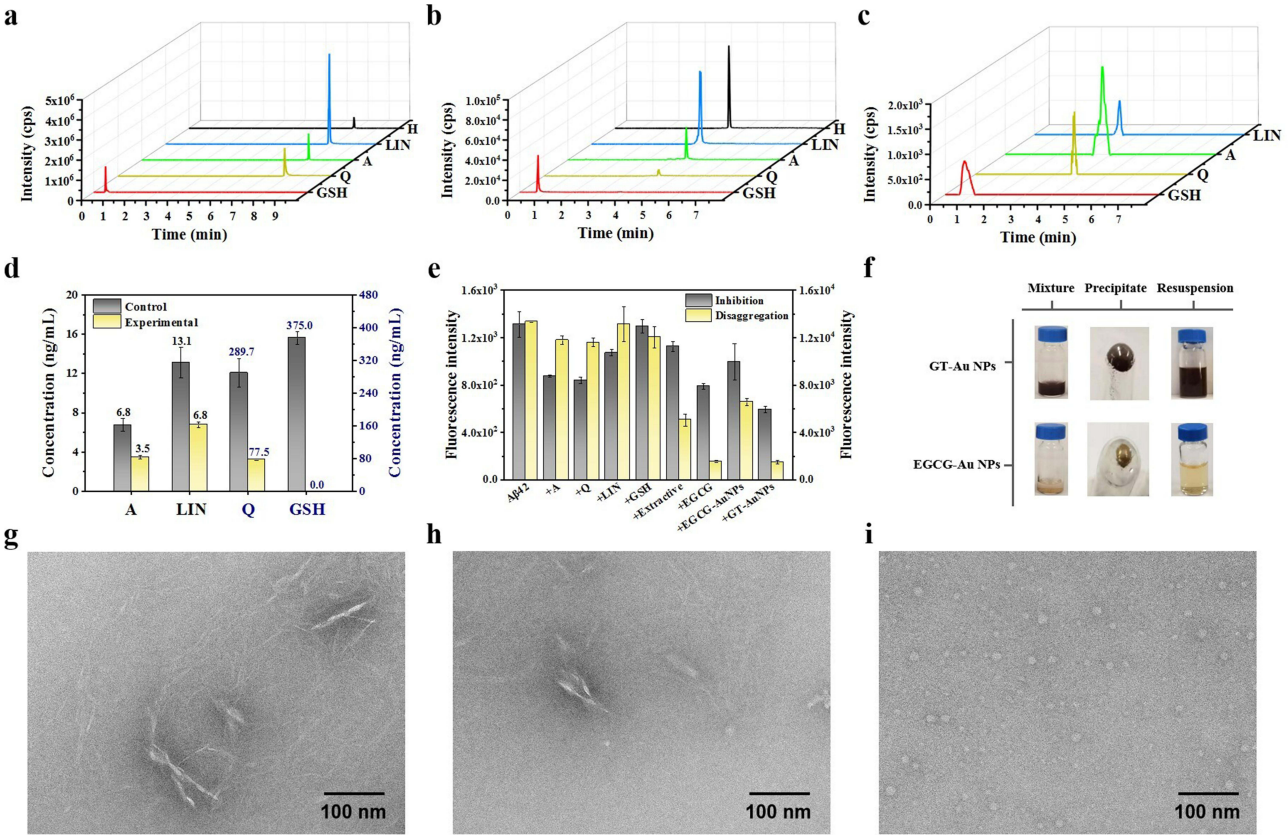

Figure 7 Comparison of GT-Au NPs and EGCG-Au NPs in terms of properties and the effects on Aβ42 fibrillation with ligand analysis. Mass spectrometry methodology development of apigenin (A), baicalin (LIN), quercetin (Q) and glutathione (GSH) in the matrix of supernatant (**a**) and GT-Au NPs precipitate (**b**). Detection of A, LIN, Q and GSH in GT-Au NPs precipitates (**c**) or post-reaction supernatants (**d**). (**e**) The effects of EGCG-Au NPs, GT-Au NPs and various small molecule ligands on Aβ42 fibrillation. (**f**) Comparison of the appearance, yield and dispersion in water of EGCG-Au NPs and GT-Au NPs. TEM images of Aβ42 in the absence (**g**) and presence of EGCG-Au NPs (**h**) or GT-Au NPs (**i**) after co-incubation for 24 h.

Table 4 Quantification Intervals and Standard Curves of Four Compounds by Two LC-MS/MS Methods

Compound	Kinetex C18 Column			Shim-Pack GIST-HP C18 Column		
	Linear Range (ng/mL)	Linear Curve	Correlation Coefficient	Linear Range (ng/mL)	Linear Curve	Correlation Coefficient
Apigenin	0.5–40	$y=6.18\ e^{-2}\ x + 0.0778$	0.9953	0.02–10	$y=1.50\ x + 0.0368$	0.9926
Quercetin	5–1000	$y=4.07\ e^{-3}\ x + 0.0537$	0.9957	0.10–100	$y=1.76\ e^{-2}\ x + 0.0102$	0.9972
Glutathione	100–10,000	$y=1.96\ e^{-4}\ x - 0.0180$	0.9967	2.50–5000	$y=3.76\ e^{-3}\ x - 0.0017$	0.9941
Baicalin	10–2500	$y=3.2\ e^{-3}\ x + 0.0952$	0.9971	0.5–2500	$y=2.92\ e^{-2}\ x + 0.0036$	0.9926

Table 5 Measured Concentrations and Reaction Rates of the Four Compounds

Compound	Group	Concentration in Control Group (ng/mL)	Concentration in Experimental Group (ng/mL)	Consumption (ng/mL)	Reaction Rate (%)
Apigenin	1:10	2.3 ± 0.2	0.8 ± 0.2	1.5 ± 0.3	65.22 ± 0.16
	1:5	4.5 ± 0.4	1.2 ± 0.2	3.3 ± 0.5	73.33 ± 0.13
	3:10	6.8 ± 0.7	3.5 ± 0.1	3.3 ± 0.7	48.53 ± 0.11
	2:5	9.0 ± 0.9	5.8 ± 0.1	3.2 ± 0.9	35.56 ± 0.10
Quercetin	1:10	96.6 ± 11.9	36.7 ± 11.9	59.9 ± 16.8	62.01 ± 0.19
	1:5	193.1 ± 23.7	49.2 ± 3.4	143.9 ± 23.9	74.52 ± 0.15
	3:10	289.7 ± 35.6	77.5 ± 4.8	212.2 ± 35.9	73.25 ± 0.15
	2:5	386.2 ± 47.4	184.7 ± 16.9	201.5 ± 50.3	52.18 ± 0.15
Glutathione	1:10	125.0 ± 5.0	0.0	125.0 ± 5.0	100.00 ± 0.06
	1:5	250.0 ± 10.0	0.0	250.0 ± 10.0	100.00 ± 0.06
	3:10	375.0 ± 15.0	0.0	375.0 ± 15.0	100.00 ± 0.06
	2:5	500.0 ± 20.0	0.0	500.0 ± 20.0	100.00 ± 0.06
Baicalin	1:10	4.4 ± 0.5	0.8 ± 0.2	3.6 ± 0.6	81.82 ± 0.16
	1:5	8.7 ± 1.0	2.7 ± 0.4	6.0 ± 1.1	68.97 ± 0.15
	3:10	13.1 ± 1.6	6.8 ± 0.3	6.3 ± 1.6	48.09 ± 0.13
	2:5	17.5 ± 2.1	11.5 ± 0.4	6.0 ± 2.1	34.29 ± 0.13

mL, and the highest response rate was 74.52 ± 0.15%. As for glutathione, the consumption increased as the substrate concentration increased, and the reaction rate was consistently 100.00%, indicating a remarkable degree of participation in the reaction, once again demonstrating its ability as a plant heavy metal detoxifier.[80]

To further investigate the role of these diverse reductants and stabilizers in green tea, we first used an aqueous solution of EGCG instead of green tea extract to synthesize the EGCG-Au NPs. Notably, the concentration of EGCG added corresponded to that of the green tea extract detected in each group, that is the initial concentrations before the reaction were 253 μg/mL, 506 μg/mL, 760 μg/mL, and 1054 μg/mL, respectively. Purified EGCG-Au NPs, GT-Au NPs, apigenin, quercetin, baicalin, glutathione, EGCG, and green tea extracts were incubated with Aβ42, and the small-molecule compounds were added at concentrations consistent with those detected in the green tea extracts.

As shown in Figure 7e, co-incubation with apigenin or quercetin reduced the fluorescence intensity in inhibition of aggregation by 33.21% (95% Confidence Interval: 23.42–42.72%) and 35.98% (95% Confidence Interval: 25.68–46.02%), and in disaggregation experiments by 11.72% (95% Confidence Interval: 7.27–16.17%) and 13.18% (95% Confidence Interval: 8.78–17.57%), respectively, as compared to Aβ42 alone, suggesting that both are effective, which is in agreement with the previous description.[9,71] Furthermore, although baicalin possessed some inhibitory effect on aggregation (18.15% decrease in intensity, 95% Confidence Interval: 7.88–28.10%), the disaggregation experiment revealed a less pronounced effect of 1.57% (95% Confidence Interval: −16.05–19.18%), whereas the opposite was

true for glutathione, which had some effect on the disaggregation experiment (9.75% decrease in intensity, 95% Confidence Interval: −1.06–20.56%), but no inhibitory effect on aggregation was found (1.18%, 95% Confidence Interval: −10.89–12.85%).

While green tea extract, as a complex mixture of components, also reached the extent of 14.19% (95% Confidence Interval: 3.07–24.96%) and 62.16% (95% Confidence Interval: 56.12–68.20%) in inhibiting aggregation and promoting disaggregation, respectively, and its internal molecules played a more positive role than the negative effects of Cu^{2+}, Zn^{2+}, etc., which promote Aβ fibrillation.[81,82] Notably, with an effectiveness of 39.86% (95% Confidence Interval: 29.65–49.83%) for inhibiting aggregation and 88.50% (95% Confidence Interval: 87.31–89.70%) for promoting disaggregation, EGCG proved to be the most effective of all the compounds, as well as of the green tea mixtures, once again demonstrating its surprising efficacy.[12]

Subsequently, we compared the effects of the EGCG-Au NPs and GT-Au NPs synthesized in this study with those of EGCG. Although the EGCG-Au NPs were able to reduce the fluorescence signals of Aβ42 by 23.98% (95% Confidence Interval: 3.01–44.63%) and 50.74% (95% Confidence Interval: 47.20–54.27%), neither of them was as effective as the EGCG aqueous solution. It is noteworthy that although the synthesized GT-Au NPs did not differ much from EGCG in Aβ42 disaggregation (88.75% reduction in fluorescence intensity, 95% Confidence Interval: 87.17–90.40%), they inhibited aggregation 1.37 times as much as EGCG with a 54.69% (95% Confidence Interval: 44.56–64.64%) reduction in Aβ fluorescence intensity. NPs have the potential to ensure in vivo stability, BBB permeability, and bioavailability, which should be further explored in subsequent experiments.

Finally, we analyzed why EGCG-Au NPs differed from GT-Au NPs. In terms of the synthesis phenomenon (Figure 7f), the synthesis of EGCG-Au NPs was characterized by a slow reaction, poor water solubility, and low yield, that is, a small amount of powder appeared at the bottom of the container only after 24 h of reaction, and there was no EGCG residue in the post-reaction supernatant of all four groups detected by LC-MS/MS. For GT-Au NPs, the solution immediately changed from light yellow to purple-red after the addition of green tea extract, and the water solubility of the particles was significantly improved, with a much higher yield than that of EGCG-Au NPs. Since the concentration of added EGCG was consistent, it is likely that other substances in green tea contributed to the differences in synthesis and effects. Thiols, such as glutathione, reducing proteins, such as thioredoxins and phytochelatins,[80,83] polyphenols, organic acids, and sugars,[84] have been shown to be involved in the detoxification of heavy metals in plants, while water-soluble modifications of hydroxyl, carboxyl, amino, and other functional groups have been achieved. TEM images directly show the effect of Au NPs on the morphological changes of Aβ42 aggregates. Pure Aβ42 samples showed typical amyloid fibrils after 24 h of incubation (Figure 7g), while the length of Aβ42 fibrils became shorter when incubated with EGCG-Au NPs (Figure 7h). Especially in the presence of GT-Au NPs, Aβ42 was mostly relatively small amorphous aggregates (Figure 7i), which is consistent with the results of CD spectra and secondary structure analysis above, suggesting that GT-Au NPs had a good effect on inhibiting Aβ42 fibrillation, which was superior to EGCG-Au NPs. To summarize, although EGCG itself is capable of reducing Au^{3+} and stabilizing the gold nucleus, this reaction proved to be difficult with a high consumption of EGCG, and the particles obtained were ineffective. In contrast, biosynthesis using cheaper green tea extracts was more efficient, and resulted in more potent functional particles that inhibited Aβ42 fibrillation.

Conclusion

In this study, we simulated the interaction of EGCG with Aβ42 by molecular docking and found that EGCG could inhibit Aβ42 fibrillation through hydrogen bonding and hydrophobic interactions. To overcome the problems of rapid metabolic clearance, low bioavailability, and poor BBB permeability of free EGCG in vivo, we demonstrated green synthesis of GT-Au NPs using green tea as a reducing and stabilizing agent. After establishing and validating the LC-MS/MS assay, the presence of EGCG around the particles was determined with a maximum reaction rate of 96.69%. It was also verified that functional small molecules, such as apigenin, quercetin, baicalin, and glutathione, which are commonly used for heavy metal detoxification and inhibition of Aβ42 fibrillation, were also stabilized around GT-Au NPs as capping ligands.

The effects of different substances on Aβ42 fibrillation were investigated using ThT fluorescence, and it was found that apigenin, quercetin, baicalein, glutathione, and even green tea extract mixtures could inhibit Aβ42 aggregation or

promote fiber disaggregation to a greater or lesser extent, but none of them were as effective as EGCG, which showed 39.86% and 88.50% inhibition of aggregation and disaggregation effects, respectively. Although the EGCG-Au NPs synthesized using EGCG aqueous solution were not as effective as free EGCG, we obtained GT-Au NPs that relied on a variety of reducing and stabilizing substances in the green tea matrix to accelerate and optimize the detoxification of heavy metals. While reducing cost, improving efficiency and enhancing water solubility, GT-Au NPs were also endowed with diversified ligand efficacy to inhibit Aβ42 aggregation, which was increased by 37.21% on top of that of EGCG. In addition to the inhibition of Aβ42 aggregation efficiency up to 54.69% relative to the incubation with pure Aβ42, the disaggregation efficiency of Aβ42 fibrils was also up to 88.75%, which is basically the same to that of EGCG. CD spectra and TEM indicated that GT-Au NPs may hinder the conformational transition to the β-sheet-rich structure of Aβ42 in aqueous solution to some extent.

Although this study is currently in the in vitro validation stage and the identification of functional substances in green tea is incomplete, which needs to be followed up with cellular or animal experiments as well as non-targeted mass spectrometry screening, we propose a promising simple and efficient drug-carrying mode that utilizes biosynthesis to confer multiple pharmacophore molecules to Au NPs, laying the groundwork for the design of new drug candidates to disrupt Aβ42 protofibrils and treat AD.

Acknowledgments

The authors are very thankful to Wuhan Sousepad Testing Technology Co., China for supporting this research. The authors extend their gratitude to Shiyanjia Lab (www.shiyanjia.com) for providing invaluable assistance in the characterization of the GT-Au NPs.

Funding

This work was financially supported by the National Key Research and Development Program of China (2023YFC3403000 and 2021YFC2401100) and Tianjin Provincial Key Research and Development Program, China (22YFYSHZ00140).

Disclosure

The authors declare no conflicts of interest in this work.

References

1. Weidner WS, Barbarino P. P4-443: the state of the art of dementia research: new frontiers. *Alzheimers Dement*. 2019;15(7S_Part_28):1473. doi:10.1016/j.jalz.2019.06.4115
2. Eisenberg D, Jucker M. The amyloid state of proteins in human diseases. *Cell*. 2012;148(6):1188–1203. doi:10.1016/j.cell.2012.02.022
3. Knopman DS, Amieva H, Petersen RC, et al. Alzheimer disease. *Nat Rev Dis Primers*. 2021;7(1):33. doi:10.1038/s41572-021-00269-y
4. Liang CQ, Li YM. Peptides for disrupting and degrading amyloids. *Curr Opin Chem Biol*. 2021;64:124–130. doi:10.1016/j.cbpa.2021.05.011
5. Mittal S, Prajapati KP, Ansari M, et al. Autooxidation of curcumin in physiological buffer causes an enhanced synergistic anti-amyloid effect. *Int J Biol Macromol*. 2023;235:123629. doi:10.1016/j.ijbiomac.2023.123629
6. Alam D, Naaz F, Islam A, et al. Role of sugar osmolytes and their nano-counterparts as inhibitors in protein fibrillation. *J Mol Liq*. 2023;386:122479. doi:10.1016/j.molliq.2023.122479
7. Borah P, Mattaparthi VSK. Insights into resveratrol as an inhibitor against Aβ1-42 peptide aggregation: a molecular dynamics simulation study. *Curr Chem Biol*. 2023;17(1):67–78. doi:10.2174/2212796817666221221151713
8. Jimenez-Aliaga K, Bermejo-Bescos P, Benedi J, et al. Quercetin and rutin exhibit antiamyloidogenic and fibril-disaggregating effects in vitro and potent antioxidant activity in APPswe cells. *Life Sci*. 2011;89(25–26):939–945. doi:10.1016/j.lfs.2011.09.023
9. Fang M, Zhang Q, Guan P, et al. Insights into molecular mechanisms of EGCG and apigenin on disrupting amyloid-beta protofibrils based on molecular dynamics simulations. *J Phys Chem B*. 2022;126(41):8155–8165. doi:10.1021/acs.jpcb.2c04230
10. Ehrnhoefer DE, Bieschke J, Boeddrich A, et al. EGCG redirects amyloidogenic polypeptides into unstructured, off-pathway oligomers. *Nat Struct Mol Biol*. 2008;15(6):558–566. doi:10.1038/nsmb.1437
11. Ahmed R, VanSchouwen B, Jafari N, et al. Molecular mechanism for the (-)-epigallocatechin gallate-induced toxic to nontoxic remodeling of Abeta oligomers. *J Am Chem Soc*. 2017;139(39):13720–13734. doi:10.1021/jacs.7b05012
12. Hyung SJ, DeToma AS, Brender JR, et al. Insights into antiamyloidogenic properties of the green tea extract (-)-epigallocatechin-3-gallate toward metal-associated amyloid-beta species. *Proc Natl Acad Sci U S A*. 2013;110(10):3743–3748. doi:10.1073/pnas.1220326110
13. Acharya A, Stockmann J, Beyer L, et al. The effect of (-)-epigallocatechin-3-gallate on the amyloid-beta secondary structure. *Biophys J*. 2020;119(2):349–359. doi:10.1016/j.bpj.2020.05.033

14. Palhano FL, Lee J, Grimster NP, et al. Toward the molecular mechanism(s) by which EGCG treatment remodels mature amyloid fibrils. *J Am Chem Soc*. 2013;135(20):7503–7510. doi:10.1021/ja3115696
15. Valverde-Salazar V, Ruiz-Gabarre D, Garcia-Escudero V. Alzheimer's disease and green tea: epigallocatechin-3-gallate as a modulator of inflammation and oxidative stress. *Antioxidants*. 2023;12(7):1460. doi:10.3390/antiox12071460
16. Liu M, Chen F, Lin T, et al. (-)-Epigallocatechin-3-gallate ameliorates learning and memory impairments by attenuating peroxidation in APP/PS1 transgenic mice. *Mol Neurodegener*. 2012;7(S1):S29. doi:10.1186/1750-1326-7-s1-s29
17. Chan S, Kantham S, Rao VM, et al. Metal chelation, radical scavenging and inhibition of $A\beta_{42}$ fibrillation by food constituents in relation to Alzheimer's disease. *Food Chem*. 2016;199:185–194. doi:10.1016/j.foodchem.2015.11.118
18. Seidler PM, Murray KA, Boyer DR, et al. Structure-based discovery of small molecules that disaggregate Alzheimer's disease tissue derived tau fibrils in vitro. *Nat Commun*. 2022;13(1):5451. doi:10.1038/s41467-022-32951-4
19. Sahadevan R, Singh S, Binoy A, et al. Chemico-biological aspects of (-)-epigallocatechin-3-gallate (EGCG) to improve its stability, bioavailability and membrane permeability: current status and future prospects. *Crit Rev Food Sci Nutr*. 2022:1–30. doi:10.1080/10408398.2022.2068500
20. Lambert JD, Lee MJ, Lu H, et al. Epigallocatechin-3-gallate is absorbed but extensively glucuronidated following oral administration to mice. *J Nutr*. 2003;133(12):4172–4177. doi:10.1093/jn/133.12.4172
21. Yang QQ, Wei XL, Fang YP, et al. Nanochemoprevention with therapeutic benefits: an updated review focused on epigallocatechin gallate delivery. *Crit Rev Food Sci Nutr*. 2020;60(8):1243–1264. doi:10.1080/10408398.2019.1565490
22. Aggarwal V, Tuli HS, Tania M, et al. Molecular mechanisms of action of epigallocatechin gallate in cancer: recent trends and advancement. *Semin Cancer Biol*. 2022;80:256–275. doi:10.1016/j.semcancer.2020.05.011
23. Dai W, Ruan C, Zhang Y, et al. Bioavailability enhancement of EGCG by structural modification and nano-delivery: a review. *J Funct Foods*. 2020;65:103732. doi:10.1016/j.jff.2019.103732
24. Lin X, Liu W, Dong X, et al. Epigallocatechin gallate-derived carbonized polymer dots: a multifunctional scavenger targeting Alzheimer's beta-amyloid plaques. *Acta Biomater*. 2023;157:524–537. doi:10.1016/j.actbio.2022.11.063
25. Yan C, Wang C, Shao X, et al. Dual-targeted carbon-dot-drugs nanoassemblies for modulating Alzheimer's related amyloid-beta aggregation and inhibiting fungal infection. *Mater Today Bio*. 2021;12:100167. doi:10.1016/j.mtbio.2021.100167
26. Istenic K, Cerc Korosec R, Poklar Ulrih N. Encapsulation of (-)-epigallocatechin gallate into liposomes and into alginate or chitosan microparticles reinforced with liposomes. *J Sci Food Agric*. 2016;96(13):4623–4632. doi:10.1002/jsfa.7691
27. Debnath K, Shekhar S, Kumar V, et al. Efficient inhibition of protein aggregation, disintegration of aggregates, and lowering of cytotoxicity by green tea polyphenol-based self-assembled polymer nanoparticles. *ACS Appl Mater Interfaces*. 2016;8(31):20309–20318. doi:10.1021/acsami.6b06853
28. John T, Adler J, Elsner C, et al. Mechanistic insights into the size-dependent effects of nanoparticles on inhibiting and accelerating amyloid fibril formation. *J Colloid Interface Sci*. 2022;622:804–818. doi:10.1016/j.jcis.2022.04.134
29. Gao G, Zhang M, Gong D, et al. The size-effect of gold nanoparticles and nanoclusters in the inhibition of amyloid-beta fibrillation. *Nanoscale*. 2017;9(12):4107–4113. doi:10.1039/c7nr00699c
30. Tapia-Arellano A, Gallardo-Toledo E, Celis F, et al. The curvature of gold nanoparticles influences the exposure of amyloid-beta and modulates its aggregation process. *Mater Sci Eng C Mater Biol Appl*. 2021;128:112269. doi:10.1016/j.msec.2021.112269
31. Kim Y, Park JH, Lee H, et al. How do the size, charge and shape of nanoparticles affect amyloid beta aggregation on brain lipid bilayer? *Sci Rep*. 2016;6:19548. doi:10.1038/srep19548
32. Sukhanova A, Poly S, Bozrova S, et al. Nanoparticles with a specific size and surface charge promote disruption of the secondary structure and amyloid-like fibrillation of human insulin under physiological conditions. *Front Chem*. 2019;7:480. doi:10.3389/fchem.2019.00480
33. Liao YH, Chang YJ, Yoshiike Y, et al. Negatively charged gold nanoparticles inhibit Alzheimer's amyloid-beta fibrillization, induce fibril dissociation, and mitigate neurotoxicity. *Small*. 2012;8(23):3631–3639. doi:10.1002/smll.201201068
34. Linse S, Cabaleiro-Lago C, Xue WF, et al. Nucleation of protein fibrillation by nanoparticles. *Proc Natl Acad Sci U S A*. 2007;104(21):8691–8696. doi:10.1073/pnas.0701250104
35. Cabaleiro-Lago C, Quinlan-Pluck F, Lynch I, et al. Inhibition of amyloid beta protein fibrillation by polymeric nanoparticles. *J Am Chem Soc*. 2008;130(46):15437–15443. doi:10.1021/ja8041806
36. Vicente-Zurdo D, Rosales-Conrado N, Leon-Gonzalez ME. Unravelling the in vitro and in vivo potential of selenium nanoparticles in Alzheimer's disease: a bioanalytical review. *Talanta*. 2024;269:125519. doi:10.1016/j.talanta.2023.125519
37. Aili M, Zhou K, Zhan J, et al. Anti-inflammatory role of gold nanoparticles in the prevention and treatment of Alzheimer's disease. *J Mater Chem B*. 2023;11(36):8605–8621. doi:10.1039/d3tb01023f
38. Sela H, Cohen H, Elia P, et al. Spontaneous penetration of gold nanoparticles through the blood brain barrier (BBB). *J Nanobiotechnology*. 2015;13:71. doi:10.1186/s12951-015-0133-1
39. Sanchis-Gual R, Coronado-Puchau M, Mallah T, et al. Hybrid nanostructures based on gold nanoparticles and functional coordination polymers: chemistry, physics and applications in biomedicine, catalysis and magnetism. *Coord Chem Rev*. 2023;480:215025. doi:10.1016/j.ccr.2023.215025
40. Rai A, Seena S, Gagliardi T, et al. Advances in the design of amino acid and peptide synthesized gold nanoparticles for their applications. *Adv Colloid Interface Sci*. 2023;318:102951. doi:10.1016/j.cis.2023.102951
41. Hou K, Zhao J, Wang H, et al. Chiral gold nanoparticles enantioselectively rescue memory deficits in a mouse model of Alzheimer's disease. *Nat Commun*. 2020;11(1):4790. doi:10.1038/s41467-020-18525-2
42. Deeths TM, Stanley RJ. Parametrial calcification in cervical carcinoma patients treated with radioactive gold. *AJR Am J Roentgenol*. 1976;127(3):511–513. doi:10.2214/ajr.127.3.511
43. Khoobchandani M, Katti K, Maxwell A, et al. Laminin receptor-avid nanotherapeutic EGCg-AuNPs as a potential alternative therapeutic approach to prevent restenosis. *Int J Mol Sci*. 2016;17(3):316. doi:10.3390/ijms17030316
44. Zhang J, Zhou X, Yu Q, et al. Epigallocatechin-3-gallate (EGCG)-stabilized selenium nanoparticles coated with Tet-1 peptide to reduce amyloid-beta aggregation and cytotoxicity. *ACS Appl Mater Interfaces*. 2014;6(11):8475–8487. doi:10.1021/am501341u
45. Liu H, Yu L, Dong X, et al. Synergistic effects of negatively charged hydrophobic nanoparticles and (-)-epigallocatechin-3-gallate on inhibiting amyloid beta-protein aggregation. *J Colloid Interface Sci*. 2017;491:305–312. doi:10.1016/j.jcis.2016.12.038

46. Alle M, Lee SH, Kim JC. Ultrafast synthesis of gold nanoparticles on cellulose nanocrystals via microwave irradiation and their dyes-degradation catalytic activity. *J Mater Sci Technol*. 2020;41:168–177. doi:10.1016/j.jmst.2019.11.003
47. Liu F, Liu X, Astruc D, et al. Dendronized triazolyl-containing ferrocenyl polymers as stabilizers of gold nanoparticles for recyclable two-phase reduction of 4-nitrophenol. *J Colloid Interface Sci*. 2019;533:161–170. doi:10.1016/j.jcis.2018.08.062
48. Vijayan A, Nair LV, Sandhyarani N. Gold cluster incorporated Rhenium disulfide: an efficient catalyst towards electrochemical and photoelectrochemical hydrogen evolution reaction. *Electrochim Acta*. 2023;446:142073. doi:10.1016/j.electacta.2023.142073
49. Atia A, Abdel-Monem YK, Salama AH, et al. Green gold@chitosan nanocomposite via solid-state synthesis; a separable catalyst for reduction of Cr(IV). *J Ind Eng Chem*. 2023;117:342–351. doi:10.1016/j.jiec.2022.10.022
50. Lee KX, Shameli K, Yew YP, et al. Recent developments in the facile bio-synthesis of gold nanoparticles (AuNPs) and their biomedical applications. *Int J Nanomed*. 2020;15:275–300. doi:10.2147/IJN.S233789
51. Li F, Qasim S, Li D, et al. Updated review on green tea polyphenol epigallocatechin-3-gallate as a cancer epigenetic regulator. *Semin Cancer Biol*. 2022;83:335–352. doi:10.1016/j.semcancer.2020.11.018
52. Choi I, Wang M, Yoo S, et al. Autophagy enables microglia to engage amyloid plaques and prevents microglial senescence. *Nat Cell Biol*. 2023;25(7):963–974. doi:10.1038/s41556-023-01158-0
53. Sun D, Li N, Zhang W, et al. Design of PLGA-functionalized quercetin nanoparticles for potential use in Alzheimer's disease. *Colloids Surf B Biointerfaces*. 2016;148:116–129. doi:10.1016/j.colsurfb.2016.08.052
54. Fujiwara H, Yoshida J, Dibwe DF, et al. Orengedokuto and san'oshashinto improve memory deficits by inhibiting aging-dependent activation of glycogen synthase kinase-3beta. *J Tradit Complement Med*. 2019;9(4):328–335. doi:10.1016/j.jtcme.2018.12.001
55. Zheng J, Xie Y, Ren L, et al. GLP-1 improves the supportive ability of astrocytes to neurons by promoting aerobic glycolysis in Alzheimer's disease. *Mol Metab*. 2021;47:101180. doi:10.1016/j.molmet.2021.101180
56. McLafferty FW. Tandem mass spectrometry. *Science*. 1981;214(4518):280–287. doi:10.1126/science.7280693
57. Zhang A, Sun H, Yan G, et al. Recent developments and emerging trends of mass spectrometry for herbal ingredients analysis. *TRAC Trends in Analytical Chemistry*. 2017;94:70–76. doi:10.1016/j.trac.2017.07.007
58. Guzzi C, Colombo L, Luigi A, et al. Flavonoids and their glycosides as anti-amyloidogenic compounds: abeta1-42 interaction studies to gain new insights into their potential for Alzheimer's Disease prevention and therapy. *Chem Asian J*. 2017;12(1):67–75. doi:10.1002/asia.201601291
59. Ferreira de Freitas R, Schapira M. A systematic analysis of atomic protein-ligand interactions in the PDB. *Medchemcomm*. 2017;8(10):1970–1981. doi:10.1039/c7md00381a
60. Gupta S, Dasmahapatra AK. Destabilization potential of phenolics on Abeta fibrils: mechanistic insights from molecular dynamics simulation. *Phys Chem Chem Phys*. 2020;22(35):19643–19658. doi:10.1039/d0cp02459g
61. Li F, Zhan C, Dong X, et al. Molecular mechanisms of resveratrol and EGCG in the inhibition of $A\beta_{42}$ aggregation and disruption of $A\beta_{42}$ protofibril: similarities and differences. *Phys Chem Chem Phys*. 2021;23(34):18843–18854. doi:10.1039/d1cp01913a
62. Mukherjee A, Sarkar D, Sasmal S. A Review of green synthesis of metal nanoparticles using algae. *Front Microbiol*. 2021;12:693899. doi:10.3389/fmicb.2021.693899
63. Barabadi H, Mobaraki K, Jounaki K, et al. Exploring the biological application of *Penicillium fimorum*-derived silver nanoparticles: in vitro physicochemical, antifungal, biofilm inhibitory, antioxidant, anticoagulant, and thrombolytic performance. *Heliyon*. 2023;9(6):e16853. doi:10.1016/j.heliyon.2023.e16853
64. Hamida RS, Ali MA, Sharif FT, et al. Biofabrication of silver nanoparticles using *Nostoc muscorum* Lukesova 2/91: optimization, characterization, and biological applications. *Int J Nanomed*. 2023;18:5625–5649. doi:10.2147/IJN.S420312
65. Nelis M, Decraecker L, Boeckxstaens G, et al. Development of a HILIC-MS/MS method for the quantification of histamine and its main metabolites in human urine samples. *Talanta*. 2020;220:121328. doi:10.1016/j.talanta.2020.121328
66. Lv C, Li Q, Liu X, et al. Determination of catecholamines and their metabolites in rat urine by ultra-performance liquid chromatography-tandem mass spectrometry for the study of identifying potential markers for Alzheimer's disease. *J Mass Spectrom*. 2015;50(2):354–363. doi:10.1002/jms.3536
67. Liu FF, Dong XY, He L, et al. Molecular insight into conformational transition of amyloid beta-peptide 42 inhibited by (-)-epigallocatechin -3-gallate probed by molecular simulations. *J Phys Chem B*. 2011;115(41):11879–11887. doi:10.1021/jp202640b
68. Warerkar OD, Mudliar NH, Momin MM, et al. Targeting amyloids with coated nanoparticles: a review on potential combinations of nanoparticles and bio-compatible coatings. *Crit Rev Ther Drug Carrier Syst*. 2024;41(2):85–119. doi:10.1615/CritRevTherDrugCarrierSyst.2023046209
69. Dourado NS, Souza CDS, de Almeida MMA, et al. Neuroimmunomodulatory and neuroprotective effects of the flavonoid apigenin in in vitro models of neuroinflammation associated with Alzheimer's disease. *Front Aging Neurosci*. 2020;12:119. doi:10.3389/fnagi.2020.00119
70. Shimazu R, Anada M, Miyaguchi A, et al. Evaluation of blood-brain barrier permeability of polyphenols, anthocyanins, and their metabolites. *J Agric Food Chem*. 2021;69(39):11676–11686. doi:10.1021/acs.jafc.1c02898
71. Ono K, Yoshiike Y, Takashima A, et al. Potent anti-amyloidogenic and fibril-destabilizing effects of polyphenols in vitro: implications for the prevention and therapeutics of Alzheimer's disease. *J Neurochem*. 2003;87(1):172–181. doi:10.1046/j.1471-4159.2003.01976.x
72. Paul PS, Patel T, Cho JY, et al. Native PLGA nanoparticles attenuate Abeta-seed induced tau aggregation under in vitro conditions: potential implication in Alzheimer's disease pathology. *Sci Rep*. 2024;14(1):144. doi:10.1038/s41598-023-50465-x
73. Ozdal ZD, Sahmetlioglu E, Narin I, et al. Synthesis of gold and silver nanoparticles using flavonoid quercetin and their effects on lipopolysaccharide induced inflammatory response in microglial cells. *3 Biotech*. 2019;9(6):212. doi:10.1007/s13205-019-1739-z
74. Bras NF, Ashirbaev SS, Zipse H. Combined in silico and in vitro approaches to uncover the oxidation and Schiff base reaction of baicalein as an inhibitor of amyloid protein aggregation. *Chemistry*. 2022;28(11):e202104240. doi:10.1002/chem.202104240
75. Li Y, Zhao J, Holscher C. Therapeutic potential of baicalein in Alzheimer's disease and Parkinson's disease. *CNS Drugs*. 2017;31(8):639–652. doi:10.1007/s40263-017-0451-y
76. Jalili S, Panji M, Mahdavimehr M, et al. Enhancing anti-amyloidogenic properties and antioxidant effects of Scutellaria baicalensis polyphenols through novel nanoparticle formation. *Int J Biol Macromol*. 2024;262(Pt 1):130003. doi:10.1016/j.ijbiomac.2024.130003
77. Simpson CA, Salleng KJ, Cliffel DE, et al. In vivo toxicity, biodistribution, and clearance of glutathione-coated gold nanoparticles. *Nanomedicine*. 2013;9(2):257–263. doi:10.1016/j.nano.2012.06.002

78. Kim HS, Lee SJ, Lee DY. Milk protein-shelled gold nanoparticles with gastrointestinally active absorption for aurotherapy to brain tumor. *Bioact Mater*. 2022;8:35–48. doi:10.1016/j.bioactmat.2021.06.026
79. Geldenhuys W, Mbimba T, Bui T, et al. Brain-targeted delivery of paclitaxel using glutathione-coated nanoparticles for brain cancers. *J Drug Target*. 2011;19(9):837–845. doi:10.3109/1061186X.2011.589435
80. Jia H, Hou D, O'Connor D, et al. Exogenous phosphorus treatment facilitates chelation-mediated cadmium detoxification in perennial ryegrass (*Lolium perenne* L.). *J Hazard Mater*. 2020;389:121849. doi:10.1016/j.jhazmat.2019.121849
81. Srivastava AK, Pittman JM, Zerweck J, et al. β-Amyloid aggregation and heterogeneous nucleation. *Protein Sci*. 2019;28(9):1567–1581. doi:10.1002/pro.3674
82. Mirzaei-Behbahani B, Meratan AA, Moosakhani B, et al. Efficient inhibition of amyloid fibrillation and cytotoxicity of alpha-synuclein and human insulin using biosynthesized silver nanoparticles decorated by green tea polyphenols. *Sci Rep*. 2024;14(1):3907. doi:10.1038/s41598-024-54464-4
83. Gupta DK, Huang HG, Yang XE, et al. The detoxification of lead in *Sedum alfredii* H. is not related to phytochelatins but the glutathione. *J Hazard Mater*. 2010;177(1–3):437–444. doi:10.1016/j.jhazmat.2009.12.052
84. Pan Z, Xie R, Chen Z. One-step simultaneous biomass synthesis of iron nanoparticles using tea extracts for the removal of metal(loid)s in acid mine drainage. *Chemosphere*. 2023;337:139366. doi:10.1016/j.chemosphere.2023.139366